UNITED STATES DEPARTMENT OF THE INTERIOR

GEOLOGICAL SURVEY

# Discussion of Ultramafic and Mafic Rocks and Platinum-Group Element Analyses from the Lost Basin Mining District, Northwestern Arizona

By

Norman J Page[1], T. G. Theodore[1] and L. A. Bradley[2]

Open-File Report 86-33

1986

This report is preliminary and has not been reviewed for conformity with U.S. Geological Survey editorial standards and stratigraphic nomenclature

1. U.S. Geological Survey, 345 Middlefield Road, Menlo Park, CA 94025
2. U.S. Geological Survey, Box 25046, DFC, Lakewood, CO 80225

Menlo Park, California

# Discussion of Ultramafic and Mafic Rock and Platinum-Group Element Analyses from the Lost Basin Mining District, Northwestern Arizona

By

Norman J Page[1], T. G. Theodore[1] and L. A. Bradley[2]

## ABSTRACT

Proterozoic amphibolite that crops out in the Lost Basin Range, Mohave County, Arizona is derived from both sedimentary and igneous protoliths. Those amphibolites derived from igneous protoliths are characterized by high Ni and Cr contents, high MgO contents, low $SiO_2$ contents and the presence of palladium and platinum. Compositions, textures and stratigraphic considerations suggest that the protoliths varied from ultramafic komatiite to basaltic komatiite to tholeiite. If these represent the actual protoliths, then this Precambrian terrane could be of interest in terms of Cu-Ni sulfide mineralization associated with komatiites.

## INTRODUCTION

The Lost Basin mining district, predominantly a gold producing one in northwestern Arizona, is located in Mohave County, 120km southeast of Las Vegas, Nevada, and about 95km north of Kingman, Arizona (Fig. 1), mostly in the Garnet Mountain 15' quadrangle east of the Gold Basin district. The Lost Basin district lies east of Hualapai Wash and west of the Grand Wash Cliffs and extends southward for a distance of 32 km from the Colorado River at the mouth of the Grand Canyon. The Proterozoic rocks in the Lost Basin Range that were mapped by Blacet (1975) and Deaderick (1980) and described by Theodore and others (1982) in detail contain occurrences of metmorphosed ultramafic and mafic rocks whose composition and platinum-group element (PGE) contents are the focus of this report.

## GEOLOGICAL SETTING

Proterozoic X rocks form most of the Lost Basin Range and consist of presumably 1,750 m.y. paragneiss and orthogneiss. In adjacent areas, coarse-grained porphyritic monzogranite of Garnet Mountain and medium-grained leucocratic monzogranite intrude the gneiss and most likely were emplaced 1,660 m.y. ago (Wasserburg and Lamphere, 1965). The rocks were regionally metamorphosed as high as upper amphibolite facies assemblages, and complexly deformed syntectonically and multiply, during the older Proterozoic X Mazatzal orogeny which occurred 1,650 to 1,750 m.y. ago (Theodore and others, 1982). Within the Lost Basin Range the Proterozoic terrance includes mappable units of migmatite, migmatitic gneiss, feldspathic gneiss, a widespread unit of variably metamorphosed quartzofeldspathic gneiss, and amphibolite. The amphibolite originated from several different protoliths. In addition, the quartzofeldspathic gneiss unit contains metaquartzite, thin lenses of marble, calc-silicate gneiss, banded iron-formation and chert. Figure 2 is a sketch map of the Lost Basin Range which shows the distribution of the major Proterozoic units and the locations of samples discussed in this report.

[1] U.S. Geological Survey, 345 Middlefield Road, Menlo Park, CA 94025
[2] U.S. Geological Survey, Box 25046, DFC, Lakewood, CO 80225

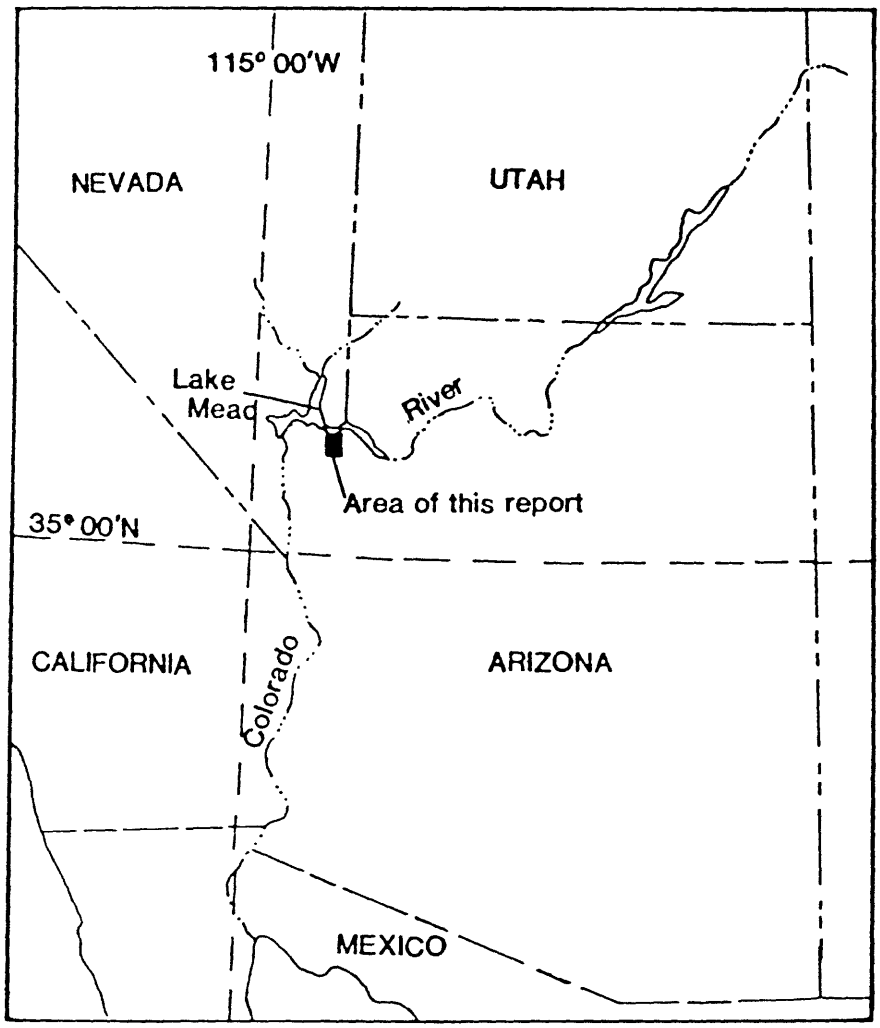


Figure 1.--Index map showing location of Lost Basin Range.

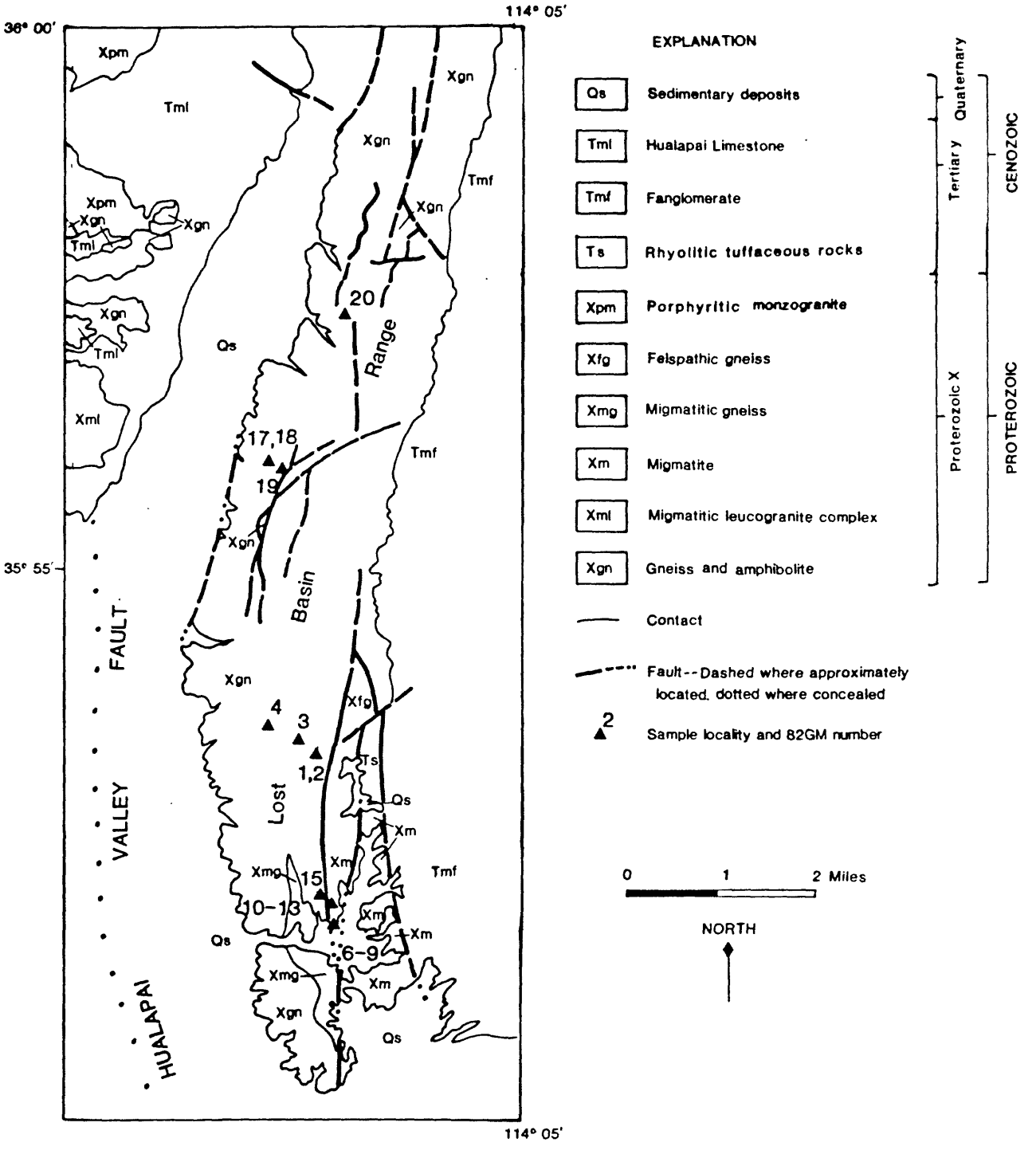


Figure 2.--Geologic sketch map of the Lost Basin Range showing locations of samples analyzed after Theodore and others (1982).

Highly deformed and lithologically complex sequences that commonly grade or change abruptly into one another across short distances are characteristic of the widespread Proterozoic X gneiss unit. Although quartzofeldspathic gneiss is the most abundant rock type in the gneiss unit, it is complexly interlayered with many other lithologies including a wide variety of pelitic schist and gneiss as well as amphibolite on the scale of an outcrop. Thick sequences of quartzofeldspathic gneiss grade by changes in proportion of the two rock types into sequences of mostly amphibolite along strike. Further, in many outcrops, there is an overall banded appearance resulting from close interlayering of quartzofeldspathic gneiss and amphibolite. Pervasive injection of the gneiss by Proterozoic X granitic magmas complicated the outcrop pattern further by producing migmatitic complexes near the southern extent of the Lost Basin Range.

Most of the metamorphic rocks contain prograde assemblages of upper amphibolite facies that have been retrograded partly or completely to greenschist assemblages as shown by Theodore and others (1982). In addition, especially near faults and gold-bearing quartz veins, propylitic, phyllitic and potassic alteration assemblages have been superimposed locally on the retrograded assemblages. Details of the petrochemistry of the rocks in the area are described by Theodore and others (1982).

The diverse kinds of gneisses probably represent a diversity of protoliths and it is by approximating the primary lithologic character of these protoliths that some aspects of the Proterozoic geologic setting may be modelled. The pelitic schists and gneisses probably represent shales and other fine-grained clastic rocks that were interbedded with graywackes with low contents of lithic volcanic detritus (Theodore and others, 1982). The graywackes are represented by the quartzofeldspathic gneiss. Locally, some carbonate-rich environments developed as represented by the minor amounts of marble and calc-silicate. Limited amounts of chert and oxide-facies banded iron formation associated with metarhyolite, all interlayered with amphibolite, suggest the development of chemical precipitates perhaps related to volcanic activity. The amphibolite represents several different protoliths including amphibolite derived from a sedimentary protolith as shown by relict beds of marble and calc-silicate minerals. However, the major portion of the amphibolite interbanded in the quartzofeldspathic gneiss probably represents basaltic (tholeiitic(?)) to andesitic igneous protoliths based on the textures, mineralogy and chemistry given in Theodore and others (1982). Other masses of amphibolite represent mafic and ultramafic protoliths as described below. Protoliths such as these inferred for rocks in the Lost Basin Range are similar to the assemblage of protoliths in other Precambrian greenstone belts except for an apparently larger volume of quartzofeldspathic material present in the Lost Basin Range than in other greenstone belts. The southern part of the range contains a greater proportion of amphibolite than the northern part.

## PETROCHEMISTRY OF THE PROTEROZOIC X AMPHIBOLITES

Amphibolite occurs in a variety of structual and stratigraphic situations in the Lost Basin Range, but most amphibolite occurs within the quartzofeldspathic gneiss unit and because of the mapping scale few of these are shown on geologic map by Blacet (1975). Lesser amounts of amphibolite occur as scattered inclusions and pendants in Proterozoic X igneous rocks. Other amphibolites crosscut lithologic layering in the enclosing gneisses and schists and locally show finer grained borders interpreted as chilled margins of dikes and sills. Amphibolites in the quartzofeldspathic gneiss unit consists of several types: (1) Fine-grained amphibolite, generally foliated, with relict cal-silicate layers that is delicately interlayered with quartzofeldspathic gneiss and is derived from a sedimentary protolith (2) foliated amphibolite that is derived from a sedimentary protolith as indicated by a significant proportion of quartz in the rock, some of which has premetamorphic as shown by relict textures (Theodore and others, 1982); (3) massive to locally foliated and layered, dense, highly magnetic, ultramafic amphibolite that usually

contains 40 to 50 volume percent of cummingtonite and that occurs as layers, lenses, and pods in the gneiss; (4) amphibolite interlayered with gneiss that was derived from a gabbroic or volcanic protolith and contains brown hornblende and plagioclase, locally with ophitic to subophitic relict textures, and abundant iron-oxide minerals; and (5) interlayered amphibolite similar to (4) but containing quartz. In addition, talc-tremolite schists and hornblendites are interlayered with the quartzofeldspathic gneiss. This report discusses types (3), (4), (5) and the sills and dikes which appear to be the most abundant types in the Lost Basin Range; the other types are discussed in detail in Theodore and others (1982).

Massive amphibolite, type (3), contains combinations of cummingtonite, plagioclase, serpentine, talc, relict clinopyroxene, hercynitic spinel, brown-semi-translucent spinel (chromite?), and magnetite. Most of the mineralogy is formed by prograde metamorphism except for perhaps serpentine and talc. Cummingtonite and serpentine form 80 to 90 percent by volume of most type (3) amphibolites. Granular to slightly foliated textures suggest serpentine developed from olivine. Locally, intergrowths of fibrous amphibole and serpentine form textures reminiscent of spinifex textures in komatiitic rocks but also could represent late fibrous amphibole replacing serpentine. Varying amounts of tremolite-actinolite, chlorite, epidote, green hornblende, carbonate and sericite are developed as retrograde metamorphic minerals. Table 1 gives whole rock, platinum-group element, and semiquantitative spectrographic analyses of amphibolites from the Lost Basin Range and whose locations are shown on figure 2; other amphibolite analyses are given in Theodore and others (1982). The relatively high Cr and Ni contents, low $SiO_2$ contents and high MgO contents confirm an ultramafic protolith for the massive amphibolites.

Amphibolite interlayered with gneiss, type (4), contains predominantly brown hornblende, plagioclase, iron oxide minerals and minor amounts of biotite as prograde metamorphic phases. One sample contained relict clinopyroxene. Brown hornblende alters to greenish hornblende and tremolite-actinolite, plagioclase to sericite, chlorite, and epidote, and biotite to chlorite during retrograde processes. Talc and carbonate are also common. Textures range from granular to foliated metamorphic ones to relict ophitic, subophitic, poikiolitic and gabbroic ones. Rocks with similar textures and mineral assemblages may also contain minor quartz and thus form type (5) amphibolites. These rocks tend to occur at the contacts of the type (4) amphibolites and biotite-hornblende-(garnet) quartzofeldspathic gneisses and may represent reaction products between the more mafic protoliths and the sedimentary protoliths. Moderate Cr and Ni contents, low $SiO_2$, MgO contents between 5 and 9 weight percent (Table 1) support a mafic protolith if not a basaltic composition protolith for type (4) and (5) amphibolites.

Dike and sills consist predominantly of calcic plagioclase and brown hornblende and have ophitic to subophitic textures and variable grain size. Biotite and iron oxide minerals are accessories. Chlorite, epidote, sericite, carbonate, and tremolite-actinolite form retrograde alteration assemblages. Textures and cross-cutting relations support a diabasic or gabbroic protolith for these rocks as does the chemistry shown in Table 1.

Most diagrams developed to discriminate among chemical compositions of extrusive and intrusive igneous rocks assume that the rock analyzed represents a magmatic liquid or at least a magmatic liquid plus crystals. Except for the dikes and sills in the Lost Mountain Range, the evidence is sparse that the chemical composition for amphibolites represent liquids. Nevertheless, because of the resemblance of the compositions to basaltic rocks, the analyses are plotted in figure 3 as weight percent MgO, $Al_2O_3$ and CaO. The diagram shows that the CaO to $Al_2O_3$ ratios approximate 1 to 1 for the type 3 amphibolites and this combined with MgO contents above 18 dry weight percent suggest that the rocks could be related to komatiites (Arndt and Nisbet, 1982b). Analyses for amphibolites given by Theodore and others (1982) and those in Table 1 were used in the plots. The amphibolite analyses recast as cation percentages and plotted on a Jensen diagram (Jensen, 1976), which has been used to classify komatiitic rocks gives a clear

Table 1: Chemical, platinum-group, and semiquantitative spectorgraphic analyses of amphibolites from the Lost Basin Range, Mohave County, Arizona. [x-ray spectroscopy by J. S. Wahlberg, A. Bartel, J. Taggart, J. Baker; FeO, $H_2O$, $CO_2$ by H. Neiman, G. Mason, J. Ryder; PGE by L. Bradley, R. Moore, J. McDade; Ag and Au by P. Briggs, R. Moore, semiquantitative analyses by L. Bradley.]

| | 82GM1 | 82GM3 | 82GM4 | 82GM6 | 82GM7 | 82GM8 | 82GM9 | 82GM10 | 82GM11 | 82GM13 | 82GM15 | 82GM16 | 82GM17 | 82GM18 | 82GM19 | 82GM20 |
|---|---|---|---|---|---|---|---|---|---|---|---|---|---|---|---|---|
| $SiO_2$ | 44.6 | 68.5 | 45.6 | 43.6 | 39.5 | 50.2 | 39.8 | 49.3 | 51.5 | 47.1 | 47.3 | 47.6 | 49.5 | 48.8 | 44.7 | 47.0 |
| $Al_2O_3$ | 16.1 | 13.2 | 9.44 | 7.63 | 6.28 | 4.43 | 5.61 | 7.06 | 5.99 | 13.9 | 16.5 | 13.5 | 6.14 | 14.1 | 12.6 | 13.8 |
| $Fe_2O_3$ | 3.73 | 2.89 | 2.09 | 4.76 | 8.44 | 3.23 | 8.17 | 1.45 | 1.78 | 3.12 | 3.29 | 3.56 | 1.27 | 4.09 | 4.89 | 4.41 |
| FeO | 10.14 | 2.83 | 6.70 | 7.41 | 7.16 | 6.90 | 6.60 | 8.14 | 9.02 | 10.78 | 7.84 | 9.12 | 7.66 | 8.22 | 11.71 | 9.89 |
| MgO | 6.60 | 1.73 | 18.8 | 21.7 | 25.2 | 20.7 | 26.0 | 18.8 | 18.9 | 6.90 | 5.49 | 7.69 | 19.2 | 8.43 | 10.8 | 6.20 |
| CaO | 9.53 | 4.72 | 10.8 | 7.44 | 5.20 | 8.77 | 4.89 | 10.2 | 9.95 | 10.4 | 14.1 | 12.0 | 11.0 | 10.4 | 9.90 | 11.3 |
| $Na_2O$ | 2.52 | 2.52 | 10.2 | 0.27 | <0.15 | 0.63 | <0.15 | 0.82 | 0.67 | 1.95 | 1.20 | 1.77 | 0.59 | 2.22 | 1.14 | 1.92 |
| $K_2O$ | 1.62 | 0.73 | 0.52 | 0.06 | 0.06 | 0.14 | 0.07 | 0.20 | 0.03 | 1.19 | 0.16 | 0.58 | 0.13 | 0.89 | 0.57 | 0.92 |
| $TiO_2$ | 1.64 | 0.37 | 0.61 | 0.67 | 0.81 | 0.60 | 0.68 | 0.08 | 0.07 | 1.63 | 1.03 | 1.30 | 0.44 | 0.98 | 0.24 | 2.14 |
| $P_2O_5$ | 0.17 | 0.10 | 0.06 | 0.06 | 0.07 | 0.08 | 0.07 | <0.05 | 0.05 | 0.15 | 0.11 | <0.10 | <0.05 | 0.10 | 0.06 | 0.19 |
| MnO | 0.23 | 0.08 | 0.22 | 0.17 | 0.24 | 0.15 | 0.22 | 0.19 | 0.20 | 0.22 | 0.19 | 0.23 | 0.24 | 0.22 | 0.45 | 0.21 |
| $H_2O+$ | 2.60 | 1.81 | 3.50 | 5.44 | 6.03 | 3.53 | 7.21 | 3.47 | 1.52 | 2.50 | 2.46 | 2.38 | 3.29 | 2.26 | 3.07 | 1.93 |
| $CO_2$ | 0.40 | 0.22 | 0.08 | 0.13 | 0.13 | 0.44 | 0.04 | 0.02 | 0.10 | 0.19 | 0.24 | 0.43 | 0.09 | 0.07 | 0.02 | 0.12 |
| Total | 100.04 | 99.88 | 99.54 | 99.56 | 99.41 | 99.91 | 99.67 | 99.85 | 99.81 | 100.20 | 100.05 | 100.33 | 99.63 | 100.88 | 100.27 | 100.19 |
| **Fire-assay-atomic absorption-emission spectrographic analyses, parts per billion** | | | | | | | | | | | | | | | | |
| Pd | 1 | 1 | 3 | 1 | 6 | 2 | 6 | 6 | 7 | 3 | 1 | 2 | 3 | 7 | 10 | 8 |
| Pt | 10 | 16 | 11 | 7 | 15 | 10 | 11 | 20 | 21 | 8 | 7 | 11 | 9 | 15 | 26 | 15 |
| Rh | <1 | <1 | <1 | <1 | <1 | <1 | <1 | <1 | <1 | <1 | <1 | <1 | <1 | <1 | <1 | <1 |
| Ir | <20 | <20 | <20 | <20 | <20 | <20 | <20 | <20 | <20 | <20 | <20 | <20 | <20 | <20 | <20 | <20 |
| Ru | <100 | <100 | <100 | <100 | <100 | <100 | <100 | <100 | <100 | <100 | <100 | <100 | <100 | <100 | <100 | <100 |
| **Semiquantitative spectrographic analyses, parts per million** | | | | | | | | | | | | | | | | |
| Mn | 1000 | 700 | 1000 | 700 | 700 | 700 | 700 | 1000 | 1000 | 1000 | 1000 | 1000 | 1000 | 1000 | 1500 | 1000 |
| Ba | 300 | 300 | 20 | 30 | 15 | 30 | 15 | 15 | 20 | 300 | 70 | 50 | 30 | 300 | 70 | 300 |
| Co | 50 | 10 | 50 | 50 | 70 | 70 | 70 | 30 | 30 | 30 | 30 | 30 | 30 | 30 | 15 | 30 |
| Cr | 70 | 3 | 2000 | 1000 | 1500 | 1500 | 1500 | 1500 | 1500 | 50 | 150 | 150 | 1500 | 300 | 300 | 70 |
| Cu | 7 | 15 | 50 | 30 | 150 | 70 | 70 | 3 | 5 | 70 | 50 | 100 | 50 | 30 | 70 | 100 |
| Nb | 10 | <10 | <10 | <10 | <10 | <10 | <10 | <10 | <10 | <10 | <10 | <10 | <10 | <10 | <10 | <10 |
| Ni | 70 | 7 | 300 | 500 | 700 | 700 | 700 | 300 | 300 | 50 | 70 | 70 | 500 | 70 | 50 | 70 |
| Pb | <10 | <10 | 15 | <10 | 10 | <10 | <10 | <10 | <10 | 10 | <10 | <10 | 15 | <10 | <10 | <10 |
| Sc | 30 | 30 | 30 | 15 | 15 | 15 | 15 | 30 | 30 | 30 | 30 | 30 | 15 | <10 | <10 | <10 |
| Sr | 150 | 200 | 20 | 15 | 30 | 15 | 30 | 7 | 10 | 200 | 150 | 150 | 15 | 150 | 30 | 150 |
| V | 200 | 70 | 150 | 150 | 150 | 100 | 150 | 150 | 150 | 200 | 300 | 200 | 100 | 300 | 200 | 300 |
| Y | 20 | 15 | 15 | <10 | <10 | <10 | <10 | <10 | <10 | 20 | 15 | 15 | <10 | 15 | 15 | 30 |
| Zr | 70 | 70 | 30 | 15 | 15 | 30 | 15 | 15 | 10 | 70 | 70 | 30 | 15 | 50 | 10 | 70 |

82GM1: Dike of amphibolite
82GM3: Finer-grained margin of dike of amphibolite
82GM4: Amphibolite type (3)
82GM6: Amphibolite type (3)
82GM7: Amphibolite type (3)
82GM8: Amphibolite or hornblendite type (3)
82GM9: Amphibolite type (3)
82GM10: Amphibolite type (3)
82GM11: Amphibolite type (3)
82GM13: Amphibolite type (4)
82GM14: Amphibolite type (4)
82GM15: Amphibolite type (4)
82GM16: Amphibolite type (5)
82GM17: Talc-tremolite schist type (3)
82GM18: Amphibolite type (5)
82GM19: Amphibolite type (4)
82GM20: Biotite-hornblende-potassium-feldspar-plagioclase-quartz gneiss

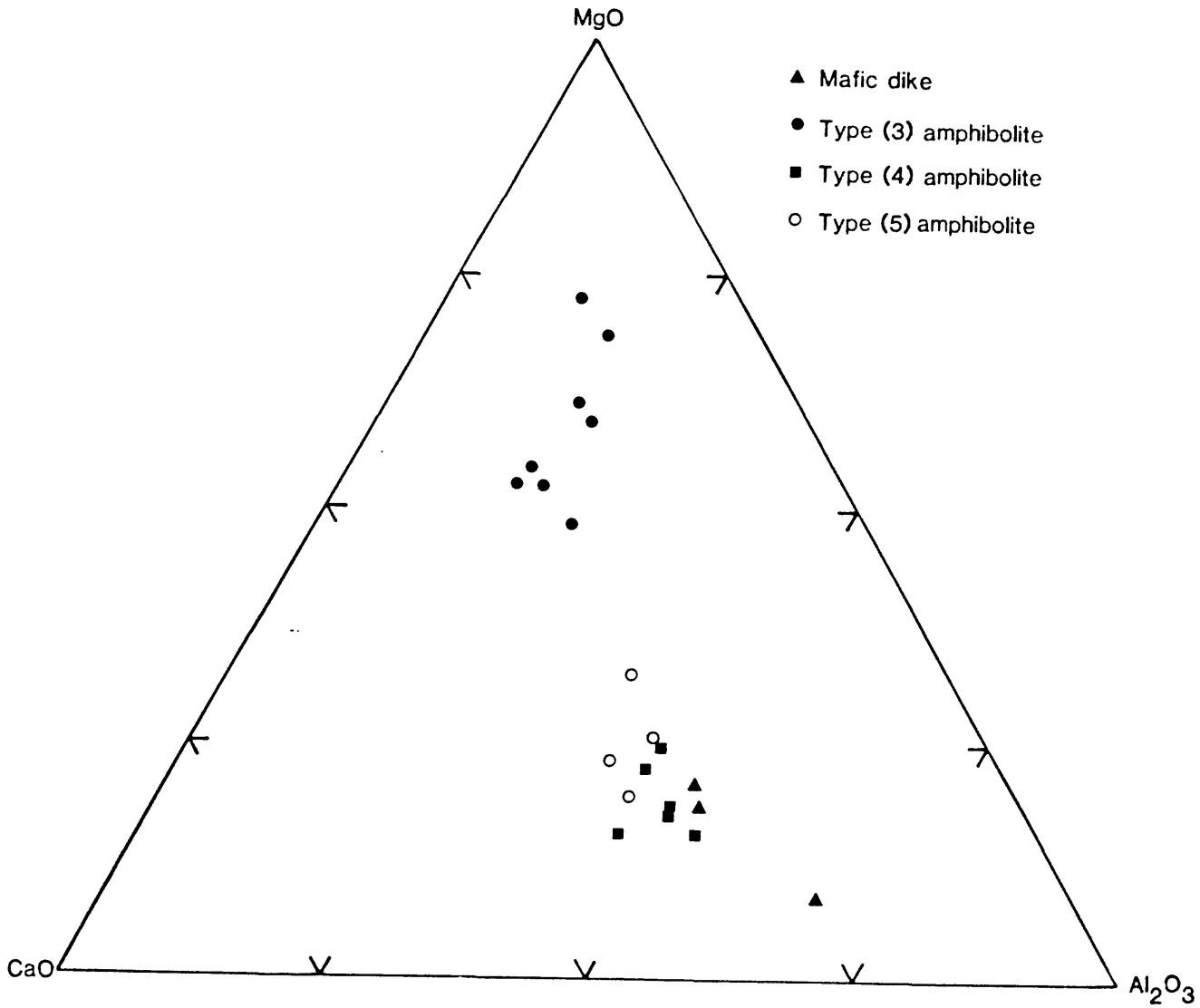


Figure 3.--Ternary diagram showing compositions of amphibolites from the Lost Basin Range in terms of weight percentage CaO, MgO, and $Al_2O_3$

picture of the variation in the amphibolite analyses with respect to MgO, $Al_2O_3$, and $FeO+Fe_2O_3+TiO_2$ (Fig. 4). Type (3), (4), (5), and dike and sill amphibolites appear to show a compositional trend from ultramafic komatiite (type 3) through basaltic komatiite and tholeiite. Of course comparison of the chemical analyses of amphibolites to other masses of chemical data on komatiites that are not as highly metamorphosed (various chapters in Arndt and Nisbet, 1982a) supports the compositional similarities including the relatively low levels of $TiO_2$ and high levels of Cr and Ni. However, as yet, the convincing textural requirements for showing that the rocks are ultramafic volcanic rocks have not been found.

## PLATINUM-GROUP ELEMENT GEOCHEMISTRY

The platinum-group element analyses in Table 1 and the seven analyses of amphibolites reported in Theodore and others (1982, Table 8, p. 82) were done by fire-assay-atomic absorption for platinum, palladium and rhodium using techniques described by Haffty and others (1977) and Simon and others (1978) and those for iridium and ruthenium by a fire-assay-spectrochemical technique described by Haffty and others (1980). These data form the basis for this discussion. Rhodium, iridium, and ruthenium contents are below the detection limits of 1, 20, and 100 ppb (parts per billion), respectively of this method. Palladium content ranges from less than 1 to 29 ppb and platinum content ranges from 7 to 33 ppb in the amphibolites; Table 2 summarizes the PGE information on the amphibolites by types. Types 4 and 5 are slightly higher in platinum and palladium on the average than type 3 amphibole. Examination and comparison of MgO content in weight percent and palladium in ppb for type 3 amphibolites suggests that samples with higher MgO contents tend to have lower palladium contents.

Average PGE contents in spinifex textured komatiites from Western Australia and Munro Township are estimated as palladium, 9.2 ppb; platinum, 8.2 ppb; iridium, 1.47 ppb; and ruthenium, 5.5 ppb by Keays (1982). These average contents of palladium and platinum are comparable with the data for type (3) amphibolites (Table 2). Keays (1982) also observed an inverse correlation between MgO content and palladium in dunitic komatiites which is similar to that observed for type (3) amphibolites. Within the range of 30 to 17 weight percent MgO, the palladium content varies from about 11 ppb to 5 ppb which is similar to the type (3) amphibolites from the Lost Basin Range. Keays (1982) also reported an average palladium content for komatiitic basalts of 15.5 and 19.3 ppb from Kambalda and Warren Township respectively that are comparable with type (4) and (5) amphibolites. Although the PGE comparison in contents are slightly different between komatiitic rocks and the amphibolites from the Lost Basin Range the overall patterns of variation appear similar.

## A POSSIBLE PROTOLITH FOR AMPHIBOLITES IN THE LOST BASIN RANGE

Three different groups of observations support the possibility that (3), (4), (5) and dikes and sills amphibolites represent tholeiitic to basaltic komatiitic to ultramafic komatiitic protoliths. The first group of observations involve the overall stratigraphic content of the Lost Basin Range which includes rocks with interpretative protoliths of quartz-rich graywacke, shale, mudstone, banded iron-formation, rhyolitic volcanic, and mafic and ultramafic rocks. These protoliths are similar to those that appear in greenstone belts elsewhere with komatiites as exemplified in a schematic cross section of the geologic setting for Western Australia (Martson and others, 1981). The second set of observations include textural indications and bulk rock compositions of the type (3), (4) and (5) amphibolites in comparison with komatiitic rocks. They appear to be similar. Thirdly, the platinum-group element geochemistry of the amphibolites compares with that of known komatiites. In conclusion, three groups of observations suggest that

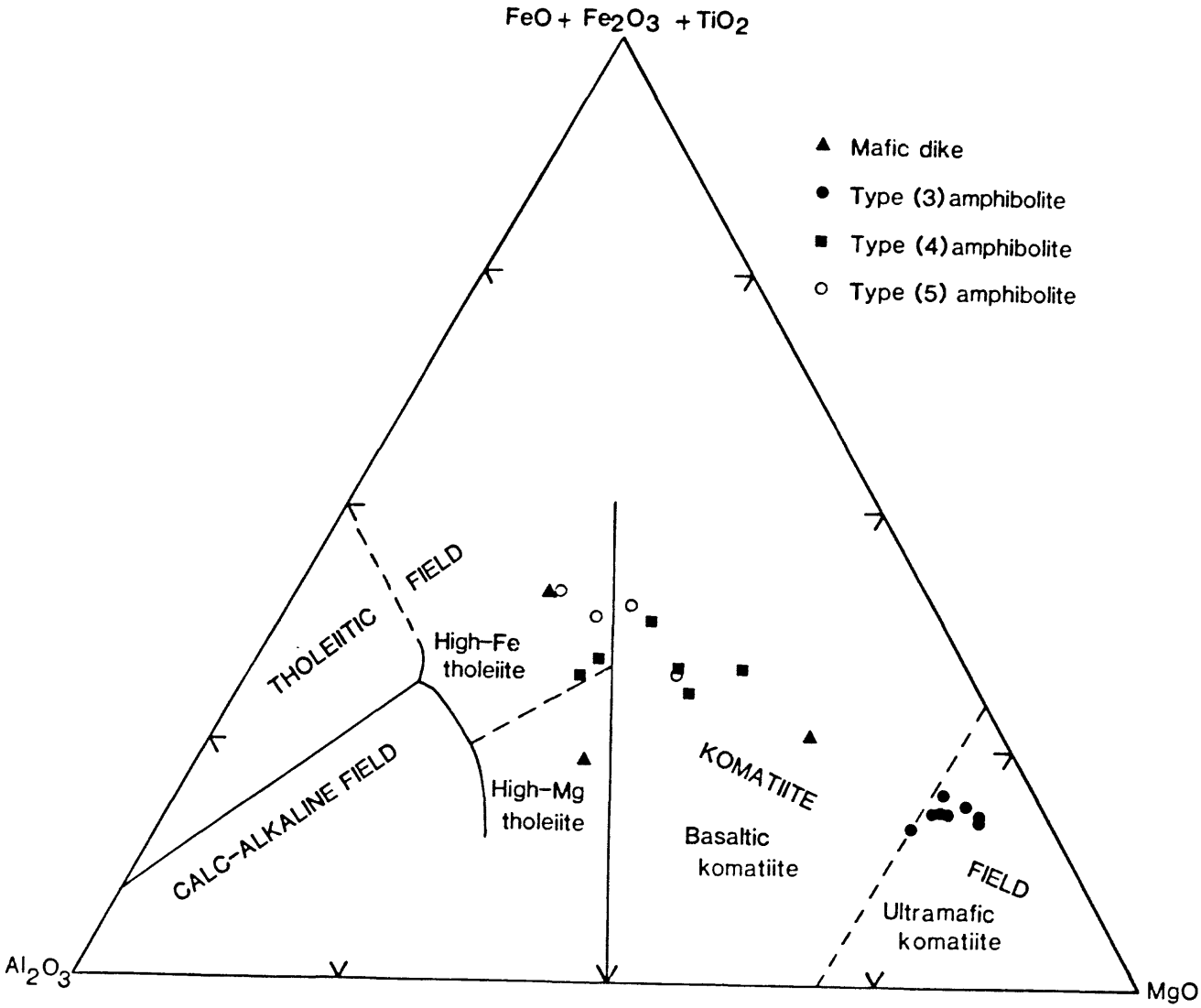


Figure 4.--Ternary diagram after Jensen (1976) showing compositions of amphibolites from the Lost Basin Range in terms of cation percentage $Al_2O_3$, MgO, and $FeO+Fe_2O_3+TiO_2$ and comparing compositions with those of komatiitic and tholeiitic rocks.

Table 2:--Summary of averages and standard deviations for palladium and platinum content in parts per billion and platinum to platinum plus palladium ratios for amphibolites from the Lost Basin Range, Arizona. $\bar{x}$=averages, $\sigma$= one standard deviation, N=number of samples with unqualified values, *Average with high value removed

| | Palladium | | | Platinum | | | |
|---|---|---|---|---|---|---|---|
| ROCK TYPE | $\bar{x}$ | $\sigma$ | N | $\bar{x}$ | $\sigma$ | N | Pt/Pt+Pd |
| All amphibolites | 5.0 | 6.1 | 21 | 16.9 | 8.0 | 24 | 0.77 |
| | 3.8* | 2.8 | 20 | | | | |
| Type (3) | 4.3 | 2.5 | 8 | 13.0 | 5.2 | 8 | 0.75 |
| Type (4) and (5) | 6.1 | 8.6 | 10 | 20.1 | 9.1 | 13 | 0.77 |
| | 3.6* | 3.1 | 9 | | | | |
| Dikes | 1.0 | - | 2 | 13.0 | - | 2 | 0.93 |

the protoliths for some amphibolites in the Lost Basin Range maybe komatiite-associated, however the appropriate field and rock textures and structures to support this contention have not yet been found. Such an assemblage suggests that this terrane in the Lost Basin Range may have the potential for Cu-Ni sulfide mineralization associated with komatiites. Further, the apparent marked increase from north to south of the amount of komatiitic protolith in the Proterozoic rocks here suggests that similar rocks may occur in fairly widespread abundances south of the Lost Basin Range.

## References Cited


Arndt, N. T., and Nisbet, E. G., 1982a, What is a komatiite in Komatiites, eds N. T. Arndt and E. G. Nisbet, George Allen and Unwin, Boston, p. 19-27.

Arndt, N. T, and Nisbet, E. G., 1982b, Komatiites; George Allen and Unwin, Boston, 526 p.

Blacet, P. M., 1975, Preliminary geologic map of the Garnet Mountain quadrangle, Mojave County, Arizona: U.S. Geological Survey Open-File Map 75-93, scale 1:48,000.

Deaderick, A. J., 1980, Geologic investigation of the Apache Oro mining claims, Lost Basin Range, Mohave County, Arizona: Unpublished report, New Mexico Institute of Mining and Technology, Socorro, New Mexico, 273 p.

Haffty, J., Riley, L. B., and Goss, W. D., 1977, A manual on fire assaying and determination of the noble metals in geological materials: U.S. Geological Survey Bulletin 1445, 58 pp.

Haffty, J., Haubert, A. W., and Page, N. J, 1980, Determination of iridium and ruthenium on geological samples by fire assay and emission spectrograph: U.S. Geological Survey Professional Paper 1129-C, pp. G1-G4.

Jensen, L. S., 1976, A new cation plot for classifying subalkalic volcanic rocks: Ontario Division of Mines Miscellaneous Paper 66, 22 p.

Keays, R. R., 1982, Palladium and iridium in komatiites and associated rocks: application to petrogenetic problems in Komatiites eds N. T. Arndt and E. G. Nisbet, George Allen and Unwin, Boston p. 435-457.

Marston, R. J., Groves, D. I., Hudson, D. R., and Ross, J. R., 1981, Nickel sulfide deposits in Western Australia: A review: Economic Geology, v. 76 p. 1330-1363.

Simon, F. O., Aruscavage, P. J. and Moore, R., 1978, Determination of platinum, palladium, and rhodium in geologic spectroscopy using electrothermal atomization: Am. Chem. Soc., Nat. Meet., 176th Miami Beach, Fla., September 11-14, 1978 (abstract).

Theodore, T. G., Blair, W. N., and Nash, J. T., 1982, Preliminary report on the geology and gold mineralization of the Gold Basin-Lost Basin mining districts, Mohave County, Arizona: U.S. Geological Survey Open-File Report 82-1052, 322 p.

Wasserburg, G. J., and Lanphere, M. A., 1965, Age determinations in the Precambrian of Arizona and Nevada: Geological Society of America Bulletin, v. 76, no. 7, p. 735-758.